Electronic structure of titanium monoxide

S. Bartkowski* and M. Neumann
Universität Osnabrück, Fachbereich Physik, 49069 Osnabrück, Germany

E. Z. Kurmaev, V. V. Fedorenko, S. N. Shamin, V. M. Cherkashenko, and S. N. Nemnonov
Institute of Metal Physics, Ural Division of the Russian Academy of Sciences, 620219 Yekaterinburg, GSP-170, Russia

A. Winiarski
Institute of Physics, University of Silesia, Uniwersytecka 4, 40-007 Katowice, Poland

D. C. Rubie
Bayerisches Geoinstitut, Universität Bayreuth, 95440 Bayreuth, Germany
(Received 27 November 1996)

The electronic structure of the monoclinic phase of titanium monoxide and a vacancy-free rock-salt phase have been investigated using x-ray photoelectron spectroscopy and x-ray emission spectroscopy techniques. For the investigation of the monoclinic structure type, polycrystalline samples of titanium monoxide were used. The samples of the vacancy-free rock-salt structure have been obtained by annealing monoclinic titanium monoxide at high temperature and pressure. The x-ray powder diffraction pattern of both types of samples revealed single-phase crystals without any substructures. The x-ray photoelectron valence band spectra reveal that the upper, mainly Ti $3d$-derived, part of the valence band is split and that the lower, mostly O $2p$-derived, band exhibits three features. A combined representation of the photoelectron valence band spectrum of the monoclinic phase and O K_α, Ti L_α, and Ti $K_{\beta 5}$ x-ray emission spectra shows that titanium and oxygen states are hybridized over almost the full valence band region, without a gap. The valence band of the vacancy-free rock-salt phase was found to be wider than that of the monoclinic phase. The experimentally obtained valence band density of states are compared with recent band structure calculations. In addition, we present spectra of the O $1s$ and Ti $2p$ core levels and show the effects of a gradual oxidation of the sample on these spectra. [S0163-1829(97)08639-6]

I. INTRODUCTION

Some of the simple binary transition metal oxides, such as TiO, VO, and NbO, are known to have a large number of vacancies in their crystal lattices. Vacancies occur in both the metal and the oxygen sublattices and even at a stoichiometric composition the number of vacancies is as high as 16% in TiO and VO and 25% in NbO. Titanium monoxide has a wide stoichiometry range. Depending on the stoichiometry, different crystal structures have been found which are all closely related to the NaCl structure. The low-temperature form of the composition $TiO_{0.9\text{-}1.1}$ has a monoclinic structure in which half of the titanium and oxygen atoms are alternately absent in every third (110) plane of the original sodium chloride lattice type.[1] In this phase the atoms in the fully occupied layers, i.e., 80% of the Ti and O atoms, have a fivefold square pyramidal coordination. Those in the vacancy-containing layers, i.e., the remaining 20% of the Ti and O atoms, are fourfold coordinated in a square planar symmetry. In a narrow composition range near $TiO_{1.25}$, a tetragonal structure was observed in which the vacancies occupy regular positions in the titanium sublattice whereas the oxygen sublattice is completely occupied.[2] The titanium atoms are octahedrally surrounded by six oxygen atoms while 80% of the oxygen atoms have five titanium ligands and 20% of the oxygen atoms have four. For a sample with an intermediate stoichiometry, $TiO_{1.19}$, a lamellar intergrowth of the monoclinic and tetragonal forms was reported.[2] The coexistence of both of these structures indicates that there is a strong preference for this material to order in these particular structures.

Early band structure calculations for TiO (Refs. 3–8), and lately Refs. 9 and 10, too, were carried out on lattices without vacancies. Schoen and Denker[11] made a step towards considering more realistic lattice types. They performed band structure calculations as a function of composition and vacancy concentration on both sublattices but did not find any vacancy induced states, even for vacancy concentrations as high as 20%. Since then numerous suggestions have been made concerning the existence and the energetic position of vacancy-induced states and the mechanism by which they stabilize the actual crystal structure. Here we can only summarize briefly a few of these suggestions. In a qualitative discussion Goodenough[12] proposed that the spontaneous creation of atomic vacancies results in a reduction of the internal energy if a gain in cation-cation binding energy exceeds the attendant loss in Madelung energy. This requirement would be fulfilled if (a) the creation of atomic vacancies reduces the lattice parameter and broadens the conduction bands so as to stabilize the occupied states in the bottom half of the bands, and (b) two electrons are trapped at each anion vacancy and two holes at each cation vacancy, thereby minimizing the loss in Madelung energy. Applying the Korringa-Kohn-Rostoker–average t-matrix formalism Huisman

et al.[13] suggested four factors which contribute to the stabilization of the defect structure: (a) Vacancies cause the mean energy of the O $2p$ band to rise and that of the Ti $3d$ band to fall. (b) The Ti $3d$-band width narrows with the vacancy concentration. (c) The vacancies generate defect states which arise in the gap between the O $2p$ and Ti $3d$ bands. (d) The Fermi level is high enough so that some of the defect states appear in the occupied part of the valence band. Based on the nonempirical Hartree-Fock-Slater method Gubanov *et al.*[14] found that anionic vacancies lead to a narrowing of the $2s$- and p-d-band widths due to the reduction of nonmetal states. Consequently, the density of metal states near the Fermi level was found to increase. Vacancy states were found well above the Fermi level with only a small admixture into the occupied part of the valence band. This resulted in a small density of electronic charge in the nonmetal vacancies and no evidence of metal-metal bonding across anionic vacancies was found. Burdett and Hughbanks[15] analyzed the TiO defect structure with the semiempirical extended Hückel method. They pointed out that the vacancy structure is not controlled by the Madelung energy and instead suggested enhanced metal-metal and metal-oxide π bonding as important factors. Subsequent band structure calculations, performed for TiO and other defect-containing titanium compounds, confirmed that anionic vacancies accommodate a considerable density of electronic charge.[10,16–21] These band structure calculations agreed with the result that the Ti $3d$ states form bonds across the anionic vacancies. The occupation of these vacancy generated bands cause the Fermi level to fall. The energetic position of the defect states and the existence of a band gap are still under discussion. References 9, 13, 15, and 20 predict that defect states completely fill the band gap, whereas defect states were only found in the occupied part of the Ti $3d$ band in Refs. 10, 19, and 21.

In the most recent band structure calculation,[22] using a self-consistent local density approximation band theory, the density of states (DOS's) of stoichiometric TiO with different vacancy concentrations and of the rock-salt phase were calculated. Among the vacancy-containing model structures TiO with about 15% vacancies is found to be the most stable phase with a rather large amount of electronic charge at the oxygen vacancy site. The shift of electronic charge into the oxygen vacancy sphere leads to (a) a reduction of the electron kinetic energy and (b) to a recovery of a part of the Madelung energy lost because of the presence of vacancies.

The role of the titanium vacancies is still largely unclear. Band structure calculations predict that the O $2p$ states are too localized to shift a significant amount of electronic charge into the titanium vacancy spheres. However, the strong correlation between the titanium and oxygen vacancy concentrations in the composition range of TiO,[23,24] and the fact that the titanium vacancies exhibit the same degree of order as the oxygen vacancies, indicates that titanium vacancies may also be of certain significance for the energetic stabilization of TiO.

To this date only a small number of x-ray and ultraviolet photoelectron spectroscopic (UPS) investigations of TiO have been published.[21,25–28] All published spectra appear to be strongly impaired either by oxidation and/or contamination of the sample surfaces, by poor sample qualities or a limited energy resolution. In agreement with some band structure calculations Wertheim and Buchanan,[26] Henrich *et al.*,[27] and Barman and Sarma[21] reported a gap in their spectra. Ichikawa *et al.*[25] performed measurements on fully oxidized samples which were prepared under atmospheric conditions. In their valence band spectra they did not find electron emission from the Ti $3d$ states at all. Kuznetsov *et al.*[28] subjected their samples to a long and intensive ion etching treatment prior to the measurements. Since the spectra of Ichikawa *et al.* and Kuznetsov *et al.* were not obtained from unperturbed surfaces they do not provide information about the electronic structure.

Most of the x-ray emission spectroscopic (XES) investigations of TiO were published in the sixties and the first half of the seventies, cf. Refs. 29–33 and references therein. At that time the spectra showed only a limited energy resolution, hence they exhibit almost no fine structure. More recent XES investigations are, according to our knowledge, not available. Because of the lack of high-quality x-ray photoelectron (XPS) and XES spectra compared with the numerous theoretical investigations, we felt that there is a real necessity to study the electronic structure of titanium monoxide experimentally using a new approach.

In this study we present the results of an investigation of the electronic structure of titanium monoxide using XPS and XES techniques. We show how a progressing oxidation of the sample influences the photoelectron spectra and analyze the electronic structure by a combined representation of the photoelectron valence band spectrum and emission spectra. From the published photoelectron spectra[21,25–28] it has not yet been possible to obtain any indication of the influence of the vacancies on the DOS of titanium monoxide. Though spectra were obtained from samples of different composition, i.e., with different vacancy contents on both sublattices,[24] the spectra exhibited mainly a change in the relative O $2p$/Ti $3d$ intensity ratio according to their particular stoichiometry.[21,27] Hence, we decided to also investigate samples without vacancies since from this type of sample the largest change in the DOS of titanium monoxide might be expected. A reduction of the vacancy content can be achieved by applying high pressure as has been shown by Taylor and Doyle[34] and Banus.[35] Depending on temperature and pressure conditions the vacancy concentration in stoichiometric TiO can be reduced to any desired concentration between 15% and zero.[34] The resulting phases were found to be stable under ambient conditions. The original vacancy concentration is restored only by reannealing at ambient pressure.[34] Elimination of vacancies does not change the physical properties significantly.[36] The superconductive transition temperature T_c raises from below 1.3 K for TiO with 15% vacancy concentration to 2.3 K for the rock-salt phase without vacancies.[37]

II. EXPERIMENT

For our measurements we have employed solid polycrystalline samples of titanium monoxide. The x-ray powder diffraction pattern of this material revealed a monoclinic crystal structure with a unit cell corresponding to the space group $C2/m$. This phase is known as α-TiO and is stable in the composition range $TiO_{0.9\text{-}1.1}$.[1,38] The parameters of the monoclinic unit cell were determined to be $a = 5.863$

TABLE I. Core level binding energies.

Core level	Binding energy (eV)[a]	FWHM (eV)
Ti $2s$	561.4	
Ti $2p_{1/2}$	460.8	1.3
Ti $2p_{3/2}$	454.7	2.0
Ti $3s$	59.1	
Ti $3p$	34.0	
O $1s$	531.4	1.1
O $2s$	23.5	

[a]Reference: $E_B(\text{Au } 4f_{7/2}) = 84.0$ eV.

± 0.003 Å, $b = 4.146 \pm 0.003$ Å, $c = 9.344 \pm 0.005$ Å, and $\beta = 107°30.31' \pm 1.00'$. The unit cell parameters are in excellent agreement with those measured by Watanabe *et al.* (who chose space group $A2/m$) for a specimen with a well-ordered array of vacant sites in the anionic and cationic sublattices.[1,23]

The vacancy-free cubic samples were prepared by annealing a finely ground powder of monoclinic TiO at a high temperature and pressure. In order to eliminate all of the vacancies from the monoclinic crystal structure the powder was subjected to a pressure of 80 kbars and was then annealed at 1665 °C for 1 min using a multianvil apparatus. The temperature was then quenched to room temperature at a rate in excess of 200 °C/sec at approximately constant pressure and then the pressure was released over a period of several hours. The x-ray powder diffraction pattern of these samples revealed a cubic unit cell corresponding to the space group $Fm3m$. The lattice parameter, calculated from the lines displayed in Fig. 8 and the (331), (420), (422), and (511) reflexes, was determined to be $a = 4.2043 \pm 0.0003$ Å.[39] The lattice parameter of the compacted samples is in good agreement with that found by Taylor and Doyle.[34] The crystal structures of both the monoclinic and cubic samples were checked by measuring survey (0.02 deg/step) and highly resolved (0.01 deg/step) XRD pattern using Cu K_α radiation in a Siemens D5000 X-ray Powder Diffractometer. The exact 2Θ positions of both types of samples were calculated by fitting the highly resolved peaks with Pearson VII, Gauss and Lorentz functions and asymmetry parameters.

The XPS measurements were obtained using a Perkin Elmer PHI 5600 ci Multitechnique System with monochromatized Al K_α radiation (FWHM = 0.3 eV). For the measurements on the monoclinic sample, the resolution of the spherical capacitor analyzer was adjusted to less than $\Delta E = 0.2$ eV and to less than $\Delta E = 0.4$ eV for the measurements on the cubic samples. In order to obtain clean surfaces for the XPS measurements the samples were fractured under UHV conditions. Since TiO exhibits metallic conductivity, the binding energies, given in Table I, were determined using the Au $4f_{7/2}$ core level [$E_B(\text{Au } 4f_{7/2}) = 84.0$ eV] as a reference.

The O K_α x-ray emission spectrum (electron transition $2p \rightarrow 1s$) was measured with a JCXA-733 electron probe microanalyzer, equipped with a fully focused Johann-type spectrometer and a TAP (Ref. 40) crystal analyzer. The O K_α spectrum was recorded in first order reflection with an energy resolution of $\Delta E = 0.5$ eV. In order to avoid any decomposition of the sample during the measurement a very soft operation mode at $U = 5$ kV and $I = 100$ nA was chosen for the x-ray tube and the position of the focused electron beam on the sample surface was changed for each scan. The Ti L_α x-ray emission spectrum (electron transition $3d4s \rightarrow 2p_{3/2}$) was recorded using an ultrasoft x-ray spectrometer with high lateral ($\Delta S = 0.5$ μm) and energetic resolution ($\Delta E = 0.8$ eV).[41] The radiation was analyzed with a diffraction grating, curved to $R = 6$ m and with $N = 600$ lines/mm. For the excitation of the x-ray emission the x-ray tube was operated at the soft settings of $U = 8$ kV and $I = 1000$ nA. The Ti $K_{\beta 5}$ x-ray emission spectrum (electron transition $4p \rightarrow 1s$) was measured using a FRS-KD-1 spectrometer, equipped with a quartz crystal analyzer.[42] The energy resolution was estimated to be $\Delta E = 0.3$ eV. The Ti $K_{\beta 5}$ x-ray emission was excited by the Cu K_α radiation of a sealed x-ray tube operated at $U = 35$ kV and $I = 50$ mA.

III. OXIDATION OF TITANIUM MONOXIDE

During the XPS measurements of several samples serious problems were encountered because of contamination of the sample surfaces by carbon and oxidation of the surfaces. Sometimes the carbon line became one of the strongest or even the most intensive line of the spectrum shortly after a sample was fractured. However, in one case the intensity of the carbon signal remained rather small for the whole period of the measurements which offered us an opportunity to observe the effects of a gradual oxidation of the sample surface almost free from carbon contamination. The experiment was performed as follows: Immediately after fracturing the sample we took spectra of all lines of the TiO spectrum. These measurements were repeated constantly while oxidation of the surface due to the pressure of residual gas progressed. After 40.75 h under UHV conditions the sample was exposed to air for 2 min and subsequently all measurements were repeated. The time which had passed after the sample was fractured is indicated at the right edge of the spectra in Figs. 2–5. The x-ray powder diffraction pattern shown in Fig. 1 reveals a perfectly monoclinic lattice structure. Photoelectron survey spectra are shown in Fig. 2. The curves $a-d$ show that the sample was only slightly contaminated with carbon and that the extent of the carbon contamination remained rather small throughout the whole period of the XPS measurements even after exposure to atmospheric conditions. The exposure to air resulted only in a strong oxidation of the sample surface.

The O $1s$ line proved to be the line which gives the best estimate for the extent of surface oxidation through the development of a shoulder at the low binding energy side of this line. The intensity of this shoulder increased with the degree of the surface oxidation as shown in the curves $a-d$ of Fig. 3. First traces of surface oxidation appeared in the O $1s$ spectrum only 15 min after breaking the sample (cf. curve a of Fig. 3). After the sample was exposed to air the O $1s$ spectrum shows clearly a superposition of two lines (curve e). The line at higher binding energy is due to bulk oxygen and that at smaller binding energy is caused by a surface layer which has been formed through the influence of the air. The comparison of curve e with curve f, which presents the O $1s$ signal of TiO_2, reveals that the electronic structure of the surface layer is similar to that of TiO_2. For comparison we also show a spectrum of TiO_2 (rutile) at the bottom of

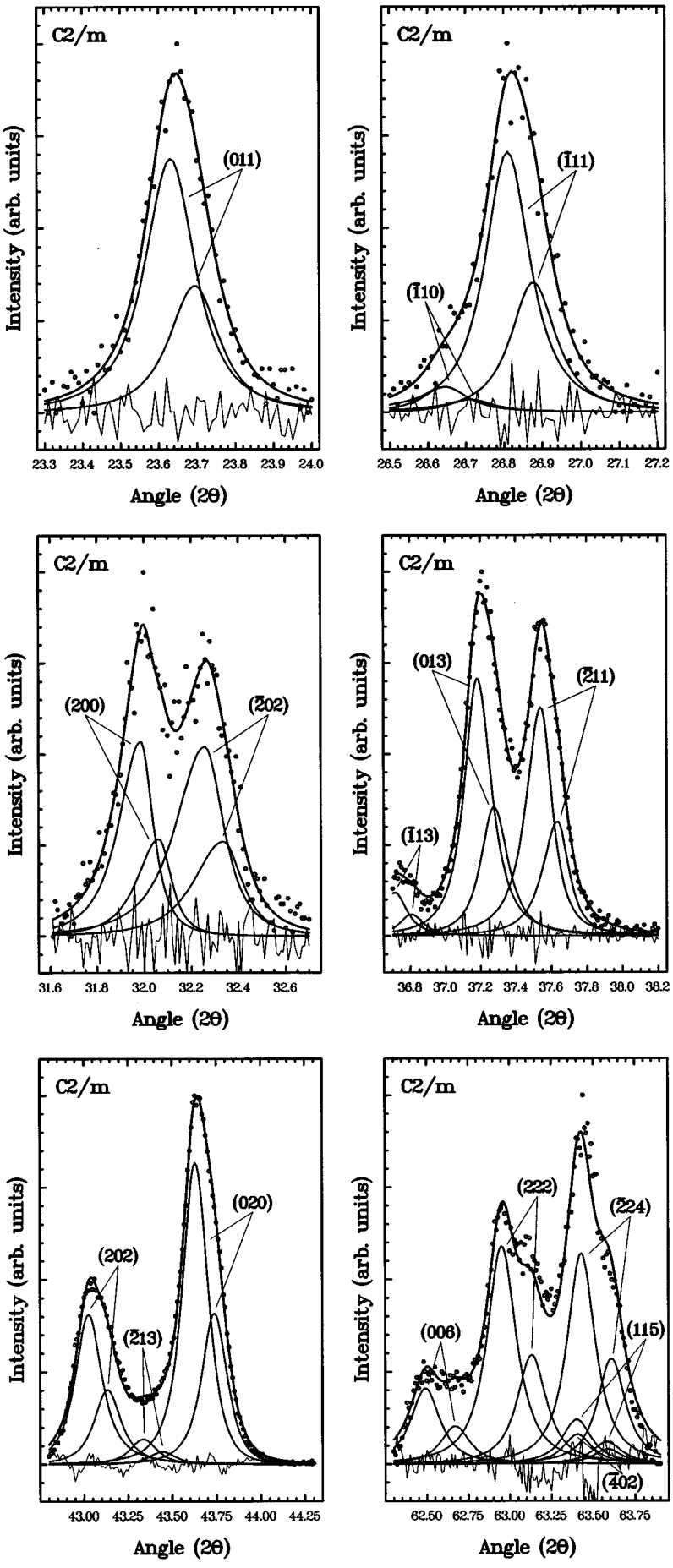

FIG. 1. X-ray powder diffraction pattern of the monoclinic sample.

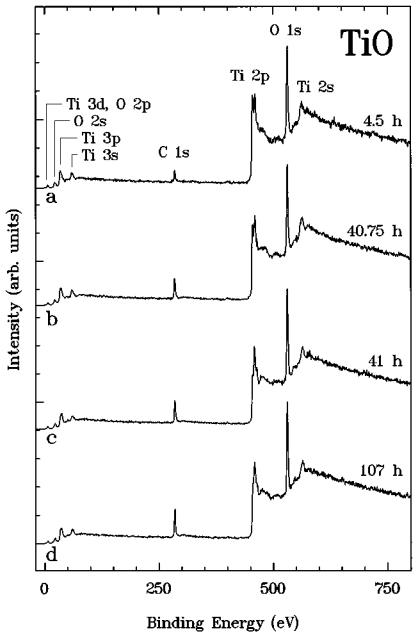

FIG. 2. Survey spectra of TiO. Spectrum *a* was obtained 4.5 h after the fracturing of the sample. The curves *b* and *c* show the spectra of the sample immediately before and after exposure to air, respectively. Curve *d* is the TiO spectrum at the end of the measurements after 107 h.

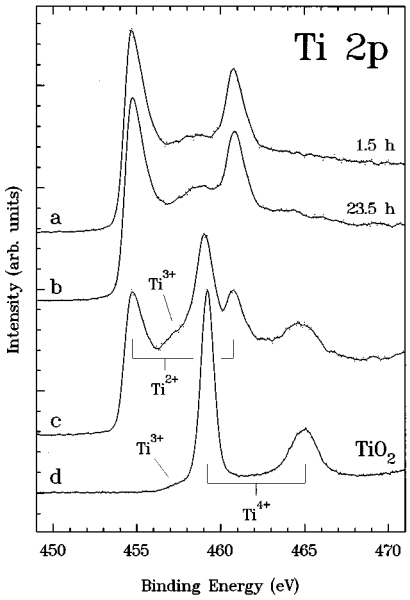

FIG. 4. Ti $2p$ spectra of TiO and TiO_2. Curve *c* shows the Ti $2p$ signal of TiO after the sample was exposed to the atmosphere. The presence of Ti^{3+} states in the Ti $2p$ doublet of TiO_2 in curve *d* arise from point defects at the sample surface.

Figs. 3–5. All of the O 1*s* signals, shown in the curves *a*-*d* of Fig. 3, exhibit a long tail of several eV's at the high binding energy side. Even the exposure of the sample to atmospheric conditions (curve *e*) had almost no effect on the tail in these spectra. That this tail is most probably due to the adsorption of water species at the sample surface is suggested by comparison with curve *g* (Fig. 3) which shows the O 1*s* signal of another sample which was treated with water under atmospheric conditions. As a result of hydration the tail developed into the most intense feature of the O 1*s* spectrum. The low binding energy feature, which is associated with a strongly oxidized sample surface (compare with curve

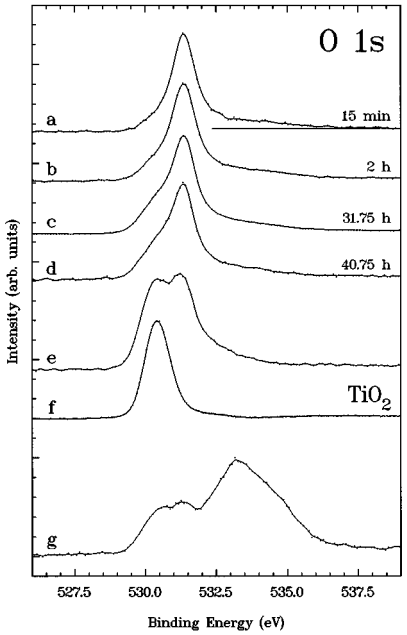

FIG. 3. The O 1*s* signals, shown in curves *a*–*d*, exhibit a prominent shoulder at the low binding energy side which increases with the degree of oxidation of the sample surface. Curve *e* shows the O 1*s* signal after the sample was subjected to atmospheric conditions. The O 1*s* signal of TiO_2 is presented in curve *f* for comparison.

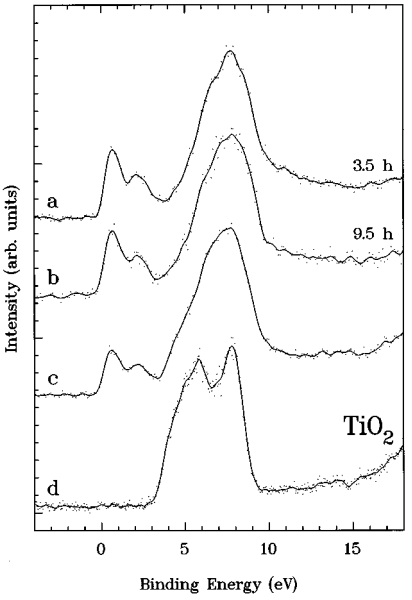

FIG. 5. Curve *a* exhibits clearly the fine structure of the TiO valence band. The gradual oxidation of the sample surface leads to the appearance of new states in the O $2p$ band and the relative density of *d* states decreases (curve *b*). These effects appeared much more pronounced after oxidation under atmospheric conditions (curve *c*). Curve *d* is the valence band spectrum of TiO_2 (rutile).

e), also developed. An unequivocal clarification of which kind of water species is adsorbed on the sample surface requires a more detailed investigation than is given here. The effects of the surface oxidation on the Ti $2p$ spectrum are illustrated in Fig. 4. Shortly after the sample was fractured, when the degree of oxidation was still small (compare with curve *b* of Fig. 3), first traces of new states could be observed at binding energies around 458–459 eV. After 1 day the intensity of these states appeared to have increased slightly (curve *b*). From the curves *c* and *d*, which show the Ti $2p$ spectra of the sample after the exposure to air and of TiO_2, respectively, it becomes evident that these features are $2p$ states arising form Ti^{4+} ions at the sample surface. After the exposure of the sample to atmospheric conditions, a complete Ti^{4+} $2p$ doublet appeared in the x-ray photoelectron spectrum. Traces of Ti^{3+} states can also be found in the curves *c* and *d*. The formation of Ti^{3+} states on defect containing TiO_2 surfaces is well known (e.g., Refs. 43–46).

The influence of the surface oxidation on the valence band spectrum is illustrated in Fig. 5. One can observe that new states, which formed as a result of the oxidation, led immediately to the disappearance of the fine structure, exhibited by the band at higher binding energies in curve *a*. The comparison of the valence band spectrum in curve *a* with those shown in the curves *b* and *c* reveals that the additional states formed mainly at the low binding energy side of this valence band feature. The two features near the Fermi level show a decrease in intensity with the degree of oxidation. Similar results were observed with ultraviolet photoelectron spectroscopy.[27] Anticipating results of the next section, in which will be shown that the upper part of the valence band includes chiefly Ti $3d$ and the band at higher binding energies mostly O $2p$ states, it becomes evident that the process which is observed in the valence band spectrum is also due to the formation of a dioxidelike surface layer. A comparison with curve *d*, which shows the valence band of TiO_2 (rutile), reveals that the position of the additional O $2p$ states in curve *c* coincides with the energetic position of the low binding energy side of the TiO_2 valence band. This part of the TiO_2 valence band is also known to contain mainly O $2p$ states.[47–49]

In Ref. 21 Barman and Sarma claimed to have measured the O $1s$ signals of their samples but, unfortunately, they did not publish these spectra. They reported that in each case the O $1s$ signals exhibited a single peak with a full width at half maximum (FWHM) of 2 eV without showing any extra features. They thus concluded that additional features, which appeared in the Ti $2p$ spectra and which were identified as the $2p$ states of Ti ions with formal oxidation states ranging from $2+$ to $4+$, were not due to a degradation of their sample but were of intrinsic character. These differently charged Ti ions were reported to reflect different local environments caused by the vacancies.

The FWHM of the O $1s$ signal of our sample, displayed in curve *a* of Fig. 3, was determined to be 1.1 eV whereas that of the oxidized sample, shown in curve *e*, is 2.1 eV. This suggests that Barman and Sarma actually performed measurements on strongly oxidized samples. This conclusion is further supported by a comparison of the Ti $2p$ and valence band spectra presented by Barman and Sarma with ours. In Fig. 4 we showed that the appearance of Ti ions with valencies higher than $2+$ is clearly a result of an oxidation process and not an intrinsic effect. Moreover, their UPS and XPS valence band spectra exhibit much stronger similarities to our spectrum of the oxidized sample, shown in curve *c* of Fig. 5, than with that shown in curve *a*. Though Barman's samples were strongly oxidized weak traces of the *d*-band splitting are present in their He II excited valence band spectra. Traces of a *d*-band splitting can also be observed in the XPS valence band spectra of Wertheim and Buchanan[26] and in the He II ultraviolet valence band spectra of Henrich and Zeiger.[27] Such a splitting did not appear in Henrich's and Barman's valence band spectra excited with He I radiation. Though Henrich mentioned that the relative photoionization cross section for the *d* states increases with the photon energy he considered the He I UP spectra to be more characteristic for the bulk. Because of the smaller mean free path of He II excited photoelectrons he attributed the weak traces of the second *d* subband to surface states. As might become apparent in Sec. IV the effect of the smaller escape depth seems to be overcompensated by the increase in the photoionization cross section.

IV. ELECTRONIC STRUCTURE OF TITANIUM MONOXIDE

A. Monoclinic phase

The x-ray photoelectron valence band spectrum and the corresponding x-ray emission spectra are shown in Fig. 6. The x-ray photoelectron valence band spectrum consists of two main bands. The low lying band, near the Fermi level, is split and extends down to 3.5 eV, approximately. The Fermi level is located at a position where this band exhibits a high density of states. The location of the Fermi level at a position with a high DOS reflects the metallic character of TiO. The metallic character manifests itself also in the asymmetric line shape (Doniach-Šunjić line shape) of the Ti $2p$ core levels (Fig. 4) which is usually found for materials with a strongly metallic character. The states of the second band, adjacent to the first band without a gap, cover the binding energy range from 3.5 eV, approximately, down to about 12 eV. This band exhibits a clear fine structure, with a distinct shoulder at the low binding energy side and a weaker one at about 8 eV. The O K_α x-ray emission spectrum reveals that this band consists mainly of O $2p$ states. The other band, above 3.5 eV, includes mainly titanium states, as is shown by the Ti L_α spectrum. According to the dipole selection rules the Ti L_α x-ray emission spectrum probes the local density of the $3d$ and $4s$ states at the titanium atom. Finally, the Ti $K_{\beta 5}$ x-ray emission spectrum shows that a Ti $4p$ partial DOS is admixed to the entire valence band region. Ti $4p$ states do even appear in the binding energy range of the O $2s$ level which reveals a noticeable O $2s$–Ti $4p$ hybridization (Fig. 7). The O K_α and Ti L_α x-ray emission spectra show that the O $2p$ states extend up to the Fermi level and that the Ti $3d$ states cover the entire binding energy range from the Fermi level down to the bottom of the mainly O $2p$-derived band. This indicates a hybridization of the Ti and O $2p$ states over almost the full valence band width.

In the photon energy region between 526 eV and 528 eV the O K_α spectrum exhibits a prominent shoulder. At the same position a feature can be found in the Ti L_α spectrum

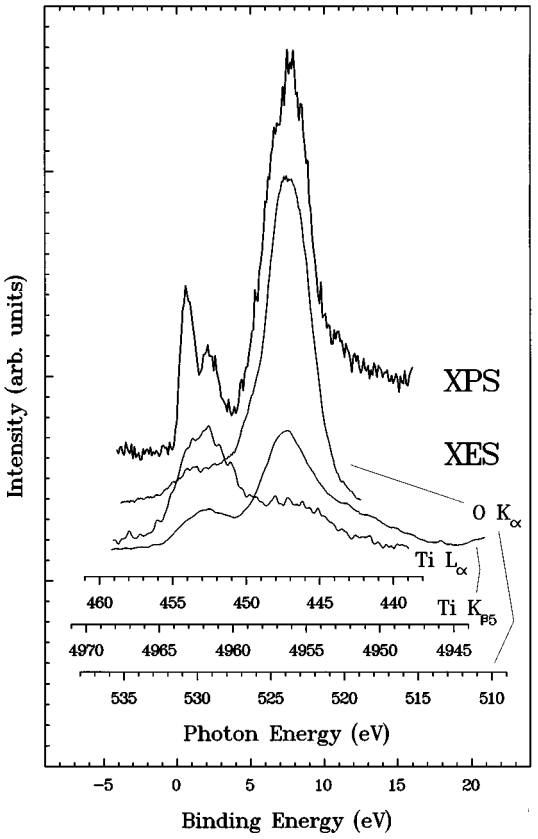

FIG. 6. X-ray photoelectron valence band spectrum and O K_α, Ti L_α, and Ti $K_{\beta5}$ x-ray emission spectra. The x-ray emission spectra resolve the total DOS of the x-ray photoelectron spectrum into the local partial O $2p$, Ti $3d4s$, and Ti $4p$ DOS's at the O and Ti sites, respectively.

around 449 eV to 451 eV. Even the Ti $K_{\beta5}$ spectrum seems to exhibit such a weak shoulder at that position. A comparison of the O K_α x-ray emission spectrum with curve *c* of Fig. 5 reveals that the shoulder in the O K_α spectrum appears at exactly the same position as that in the x-ray photoelectron valence band spectrum of the oxidized sample. Since XES is a much more bulk sensitive technique than XPS we are certain that the shoulder in the O K_α spectrum reflects a real feature of the O $2p$ bulk DOS and is not due to a surface effect.

The splitting of the $3d$ band could not be reproduced in the Ti L_α x-ray emission spectrum. However, the two features of the mainly Ti $3d$-derived band are reflected by a distinct shoulder and by the intensity maximum of the Ti L_α spectrum at photon energies of about 454.5 eV and 453.0 eV, respectively. Near the Fermi level, self-absorption becomes a dominating effect in x-ray emission spectra of samples with a metallic character.[50] Hence, the intense spectral feature at the Fermi level of the photoelectron spectrum appears considerably attenuated in the Ti L_α spectrum. Although self-absorption influences the spectral intensity, it has no effect on the L_α emission edge or on the fine structure beyond the edge, as was shown by Holliday.[29] Immediately below the Fermi level the O K_α spectrum shows a feature which coincides with the Ti $3d$ subband at the Fermi level. As in the case of the Ti L_α spectrum the intensity of this feature might

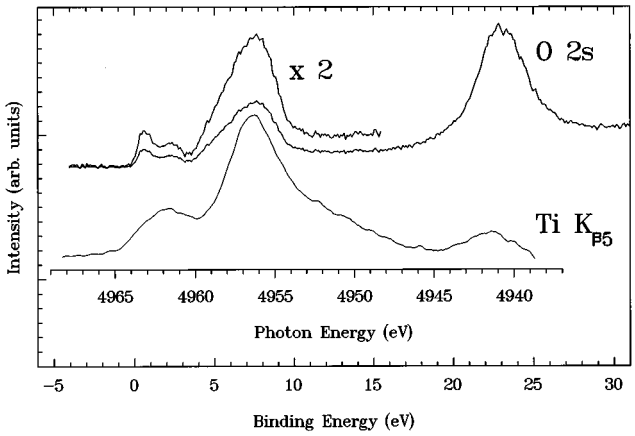

FIG. 7. Distribution of the Ti $4p$ partial DOS in the valence band region. The Ti $K_{\beta5}$ x-ray emission spectrum reveals a hybridization of Ti $4p$ and O $2s$ states.

also appear attenuated through self-absorption. In the energy range of the second Ti $3d$ subband, at binding energies between 1.0 eV and 3.5 eV, the O K_α spectrum exhibits no corresponding feature. This means that this subband is either free of O $2p$ states or at least strongly dominated by a $3d$ partial DOS. This result is also in agreement with Henrich's and Barman's ultraviolet photoelectron spectra.[21,27] With He I excitation these spectra exhibit only an intense feature at the Fermi level. For this wave length the ratio of the O $2p$/Ti $3d$ photoionization cross sections is 2.1.[51] Hence the spectra are governed by the O $2p$ DOS. Only excitation with He II photons, for which the O $2p$/Ti $3d$ photoionization cross section ratio decreases to 1.7, leads to the appearance of traces of the second $3d$ subband. Finally, for Al K_α radiation the total photoionization cross sections are smaller by four orders of magnitude and the ratio has further decreased to 1.4. Because of the much smaller photoionization cross sections the resolution is much better than in the UPS regime and the intensity ratio of the Ti $3d$ subbands has further shifted in favor of the lower band. Thus, considering the ultraviolet photoelectron spectra of Henrich and Barman together with our x-ray photoelectron valence band spectrum we can also construct a logical line of arguments that lead to the same conclusion as the findings of the x-ray emission spectra. In the discussion above we have neglected the influence of transition matrix element effects. Since single crystalline titanium monoxide does not exist, photoelectron emission always originates from a huge number of tiny, randomly orientated single crystalline particles (size $\approx 1\,\mu$m). Thus transition matrix element effects average out largely and the ultraviolet photoelectron spectra in Refs. 21 and 27 can only have been obtained in quasi-angle-integrated measurements. Hence, one can omit the consideration of transition matrix element effects for the above discussion and discuss ultraviolet photoelectron spectra of titanium monoxide only on the basis of photoionization cross sections. In Ref. 27 Henrich *et al.* already presumed that transition matrix element effects did not appear to play a major role in his He I and He II excited photoelectron spectra and that the shape of his spectra appeared to be dominated by the relative change in the photoionization cross section, but he was unable to justify his presumption.

B. Cubic phase

Figure 9 displays the spectra of two samples, denoted by *A* and *B*, from which the vacancies have been eliminated. Figure 8 gives an unequivocal proof of the cubic structure of these samples. Since the samples were prepared from a finely ground powder, contamination and oxidation effects appear stronger than for the polycrystalline samples which were fractured under UHV conditions. The survey spectra in Fig. 9 (upper panel, left) reveal a serious carbon contamination of sample *A* which caused some features to emerge in the valence band spectrum (upper panel, right) at binding energies higher than about 10 eV. From the O 1*s* and Ti 2*p* core level spectra in Fig. 9 it becomes apparent that sample *A* is also stronger oxidized than sample *B*. However, the oxidation effects and the carbon contamination did not obscure the characteristic features of the bulk DOS.

As is obvious from Fig. 9 the total valence band DOS strongly resembles that obtained from the monoclinic phase. As in the case of the monoclinic sample the valence band fine structure exhibits clearly a splitting of the Ti 3*d* band. The shoulder which appeared at the low binding energy side of the O 2*p* band of the monoclinic sample (compare with curve *a* of Fig. 5) appears to be absent in the valence band spectrum of the cubic phase (cf. sample *B*). The shoulder in the valence band of sample *A* is most probably due to the strong oxidation of the sample. In contrast to the monoclinic sample the shoulder at the high binding energy side of the O 2*p* band (marked by an arrow) appears more intense in the valence band spectra of both cubic samples. However, though the relative photoionization cross section for the O 2*p* states is about 24 times higher than for the C 2*p* states,[51] one must take into consideration that the shoulder might also be influenced to a small extent by carbon-induced features.

C. Comparison with band structure calculations

For the comparison of theoretically obtained valence band DOS's with the experimental spectra only the latest band structure calculations were taken into consideration (Fig. 10). The curves *a* and *b* show the spectra of the monoclinic sample and of the cubic sample *B*, respectively. The curves *c* and *e*, taken from Hörmandinger *et al.*,[10] show the total DOS's of TiO without vacancies and of a defect structure with 15% vacancies randomly distributed in each sublattice ($Ti_{0.85}O_{0.85}$), respectively. Curve *d* presents the total DOS of $TiO_{0.75}$ calculated by Schlapansky *et al.*[19] For this band structure calculation a sodium chloridelike lattice was assumed with an ordered array of 25% vacancies in the oxygen sublattice. The DOS shown in curve *f* was obtained by Hobiger *et al.*[20] for TiO for which the NbO structure was assumed. The NbO structure comprises 25% vacant lattice sites in ordered positions in each sublattice.

In general, the band structure calculations show that the widths of the DOS's narrow with the number of vacancies in the applied structure models. While the widths of the curves *c* and *d* are in good agreement with the experimental spectra, those of the curves *e* and *f* are too small. In comparison with curve *a* the $Ti_{0.75}O_{0.75}$ DOS is too small by more than 3 eV's. Our experimental results seem to verify qualitatively the shrinkage of the valence band widths with the number of vacancies. The total valence band width of the monoclinic sample was determined to be about 1 eV smaller than the valence band width of the vacancy-free cubic sample. This result supports the idea of the existence of vacancy states.

The band structure calculations predict a gap between the two main bands. The gap widths were also found to narrow with the number of vacancies in the model structures and vanished only if $Ti_{0.75}O_{0.75}$ is reached. Though a content of 25% vacant lattice sites in each sublattice exceeds greatly that of real TiO, the absence of a band gap and the prediction of the Fermi level at a position where the DOS is high matches the experimental results. However, from the experimental spectra it is apparent that neither the x-ray photoelectron or emission spectra of the monoclinic sample nor the photoelectron spectra of the cubic samples supply any indication of a gap.

The curves *d* and *f* agree with the experimental spectra in that they show a splitting of the Ti 3*d* band although the energetic separation of the *d*-band features is too small. The splitting of the *d* band appears only if the model structure contains vacancies. The DOS of the vacancy-free model structure in curve *c* shows an almost linearly increasing and featureless *d*-band DOS towards the Fermi level which is not in agreement with the experimental results. Since the valence band spectra of both the monoclinic sample and of the vacancy-free samples exhibit a *d*-band splitting the splitting cannot be due to vacancy-induced effects as suggested by the band structure calculations.

The spectral features which have been found in the 2*p* bands are reproduced qualitatively in the curves *c*, *d*, and *e*. As in the valence band spectrum of the monoclinic sample the $TiO_{0.75}$ and $Ti_{0.85}O_{0.85}$ DOS's exhibit prominent shoulders at the low binding energy side of the 2*p* bands. In curve *c*, which was calculated for TiO without vacancies, considerable spectral weight emerges at the high binding energy side of the O 2*p* band. This result is in agreement with the shoulders which were found in the O 2*p* spectra of both cubic samples. In the TiO, $TiO_{0.75}$, and $Ti_{0.85}O_{0.85}$ band structure calculations O 2*p* partial DOS's were found in the entire Ti 3*d*-derived band.[10,19] Only the $Ti_{0.75}O_{0.75}$ band structure calculation predicted a weak admixture of O 2*p* states to the Ti 3*d* subband at the Fermi level.[20] In agreement with the experimental results all band structure calculations predicted the Ti 3*d*–O 2*p* hybridization over the full width of the mainly O 2*p*-derived band. The Ti $K_{\beta 5}$ double peak structure, as shown in Fig. 6, has been reproduced by the $Ti_{0.85}O_{0.85}$ and $Ti_{0.75}O_{0.75}$ band structure calculations. The latter could even reproduce the admixture of Ti 4*p* states to the O 2*s* band. Detailed analyses of the bonding situation of $TiO_{0.75}$ and $Ti_{0.75}O_{0.75}$ are given in Refs. 19 and 20. In these band structure calculations it was found that Ti 3*d* states extend into the oxygen vacancy spheres and form bonding states across the oxygen vacancies. The main DOS contribution arising from vacancy-induced states led to the filling of the band gap in $Ti_{0.75}O_{0.75}$ and appeared immediately above the gap in the $TiO_{0.75}$ band structure calculation. In the energy region where, according to Ref. 20, vacancy states should occur the Ti L_α and O K_α x-ray emission spectra reveal some features which appear to indicate a *d*-*p* hybridization. Since a feature similar to the 450-eV feature of the Ti L_α spectrum has also been found in the Ti L_α spectrum of

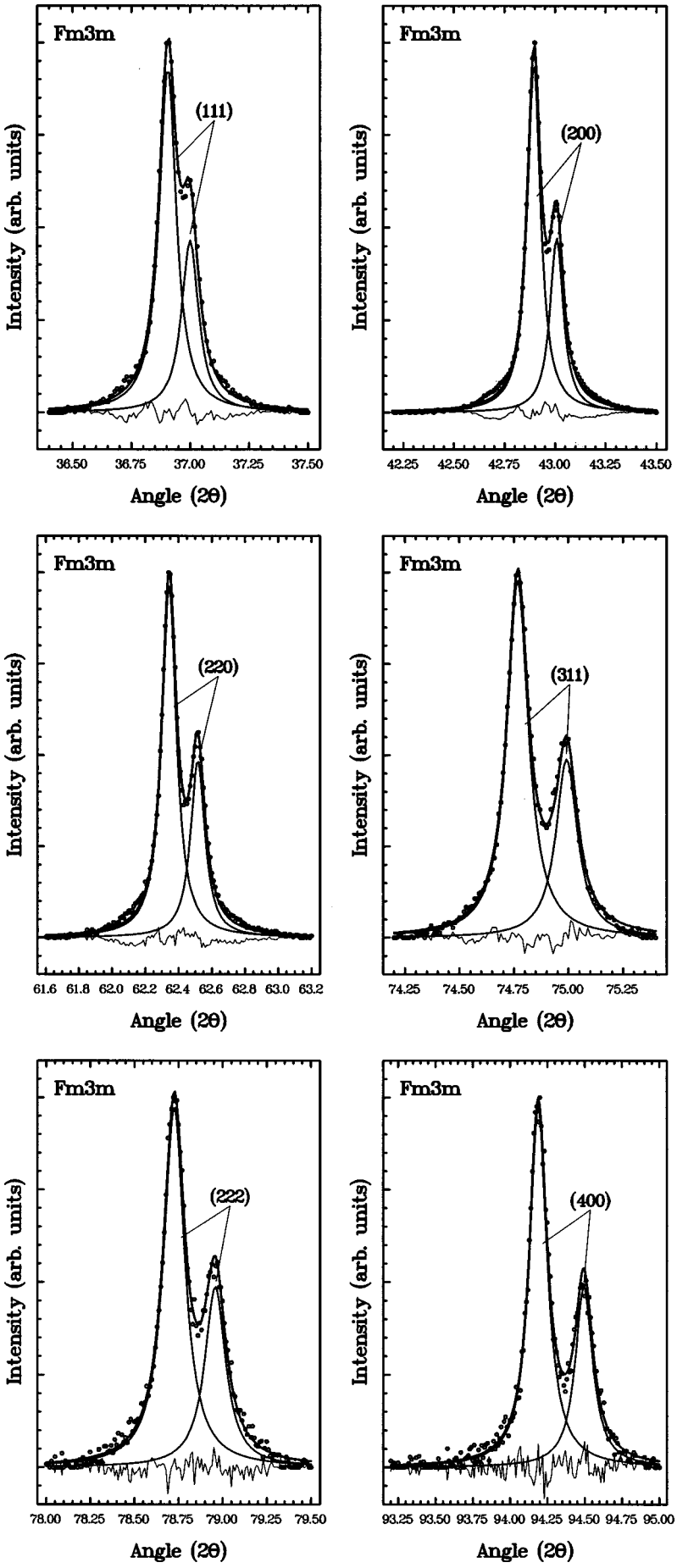

FIG. 8. X-ray powder diffraction pattern of cubic TiO.

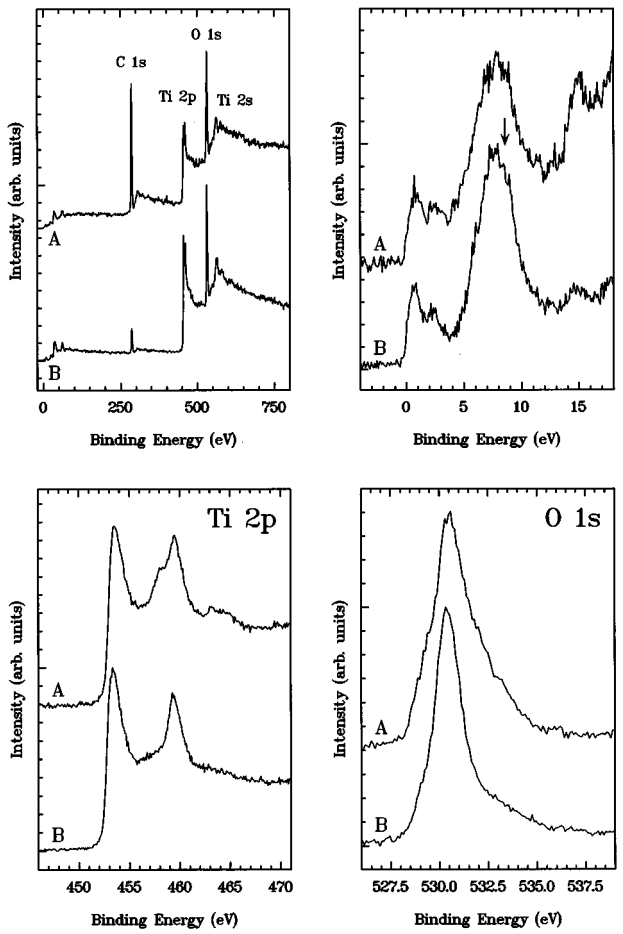

FIG. 9. X-ray photoelectron spectra of the vacancy-free cubic phase.

pure titanium[31,32,50] it is rather uncertain whether this feature can be attributed to vacancy states or to a d-p hybridization or whether it is characteristic for TiO at all.

In a recent study of the early transition metal oxides TiO was classified in the Mott-Hubbard regime ($U<\Delta$), based on CI cluster calculations and satellites which are believed to attend the Ti $2p$ core lines.[52] From the CI cluster calculations a large charge-transfer energy of $\Delta=8.0\pm1.0$ eV and a d-d Coulomb and exchange energy of $U=3.5\pm0.5$ eV were obtained.

We classify TiO as a d-band metal with a correlation energy U smaller than the d-band width W.[53] Our Ti $2p$ spectrum (curve a of Fig. 4) does not exhibit any indication of satellite structures. The high metallic conductivity of TiO proves that a d-d gap does not exist. This is also confirmed by numerous band structure calculations and by the bremsstrahlung isochromat spectra presented by Barman and Sarma[21] and also by the Doniach-Šunjić line shape of the Ti $2p$ core lines (Fig. 4).

The measured d-band width of cubic TiO is in full agreement with the calculated (linear augmented plane wave) DOS obtained by Hörmandinger *et al.*[10] (curve c of Fig. 10) and also with those obtained by Leung *et al.*[22] and Ahuja *et al.*[54] Leung *et al.* performed a full relaxation of the crystal structure using a damped version of the variable cell shape molecular-dynamics method. The valence band DOS of Ahuja *et al.* was obtained by a first-principles total-energy

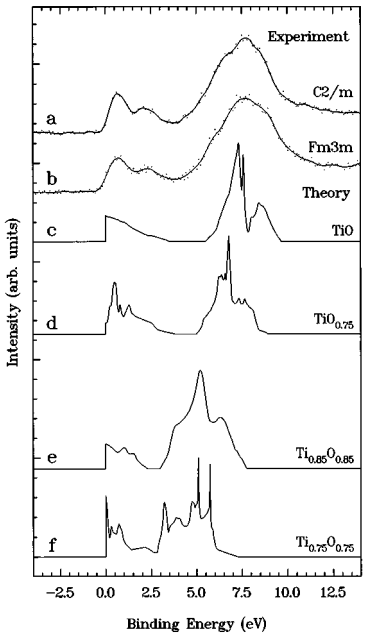

FIG. 10. Comparison of the experimental valence band DOS's with those obtained by some of the latest band structure calculations for different model structures (Refs. 10, 19, and 20).

calculation using the full potential linear muffin-tin orbital method. Whereas curve c shows an almost featureless d band the DOS's obtained by Leung *et al.* and Ahuja *et al.* exhibit a pronounced feature immediately below the Fermi level, similar to that observed in the experimental spectrum. However, the second d-band peak could not be reproduce by these band structure calculations.

A splitting of the d band into a coherent and incoherent part as a function of U/W, as observed for other Ti and V oxides,[55,56] seems to be unlikely. For the strongly correlated compounds in Refs. 55 and 56 the coherent part of the single-particle spectral functions are distinctly smaller than the experimentally observed d-band widths (cf. Fig. 2 of Ref. 55). Since for the rock-salt phase of TiO the calculated[10,22,54] and measured d-band widths are equal, the entire experimentally obtained d-band must be attributed to the coherent part of the single-particle spectral function. The comparison of the measured valence band spectrum and band structure calculations of cubic TiO with those shown in Fig. 2 of Ref. 55 reveals that TiO can most appropriately be compared with ReO_3 with $U\ll W$. This result gives additional confirmation to the classification of TiO in the d-band metal regime.

V. SUMMARY

In this study we presented an investigation of the electronic structures of the monoclinic and cubic phases of titanium monoxide by x-ray photoelectron and x-ray emission spectroscopy. We have demonstrated the effects of a gradual oxidation of the sample surface on the photoelectron spectra. These observations enabled intrinsic and extrinsic spectral features to be distinguished. The most prominent effects of the surface oxidation occurred in the O $1s$ spectrum where it leads to the formation of a distinct shoulder at the low binding energy side of the O $1s$ line. In high-energy resolved

photoelectron valence band spectra we show the valence band fine structures of both phases. The valence band spectra of both phases reveal a splitting of the Ti $3d$ band. This rules out that the splitting is a vacancy-induced effect as suggested by the band structure calculations. Significant differences have been found in the DOS's of the O $2p$ bands of both phases. This result and the existence of O $2p$ states at the Fermi level indicate that the electronic structure of TiO is strongly influenced by O $2p$ states which appear to be rather delocalized. The Ti L_α, O K_α, and Ti $K_{\beta 5}$ x-ray emission spectra reveal that titanium and oxygen states are hybridized over almost the entire valence band width. The Ti $K_{\beta 5}$ spectrum reveals also a hybridization between Ti $4p$ and O $2s$ states.

Only a limited agreement was found when comparing the total DOS's of the latest band structure calculations with the experimental valence band spectra. In contrast to the predictions of numerous band structure calculations neither the valence band spectrum of the monoclinic nor those of the cubic samples exhibit a gap. For cubic TiO we found a larger total valence band width than for TiO having a monoclinic lattice structure. This finding is in agreement with the predictions of band structure calculations. The predictions of numerous band structure calculations concerning the existence of vacancy states could not be directly verified by our experiments but the smaller total valence band width of monoclinic TiO supports such predictions.

ACKNOWLEDGMENTS

Financial support by the Deutsche Forschungsgemeinschaft (DFG), the Russian Foundation for Fundamental Research (Grant No. 96-03-32092) and the NATO International Scientific Exchange Program (Project No. HTECH LG 940861) is gratefully acknowledged.

*Electronic address: SBARTKOWSKI@fb4-301.physik.uni-osnabrueck.de

[1] D. Watanabe, J. R. Castles, A. Jostsons, and A. S. Malin, Acta Crystallogr. **23**, 307 (1967).
[2] D. Watanabe, O. Terasaki, A. Jostsons, and J. R. Castles, J. Phys. Soc. Jpn. **25**, 292 (1968).
[3] H. Bilz, Z. Phys. **153**, 338 (1958).
[4] J. Yamashita, J. Phys. Soc. Jpn. **18**, 1010 (1963).
[5] V. Ern and A. C. Switendick, Phys. Rev. **137**, A1927 (1965).
[6] J. M. Honig, W. E. Wahnsiedler, and J. O. Dimmock, J. Solid State Chem. **5**, 452 (1972).
[7] L. F. Mattheiss, Phys. Rev. B **5**, 290 (1972).
[8] A. Neckel, P. Rastl, R. Eibler, P. Weinberger, and K. Schwarz, J. Phys. C **9**, 579 (1976).
[9] K. Schwarz, Phys. Chem. Miner. **14**, 315 (1987).
[10] G. Hörmandinger, J. Redinger, P. Weinberger, G. Hobiger, and P. Herzig, Solid State Commun. **68**, 467 (1988).
[11] J. M. Schoen and S. P. Denker, Phys. Rev. **184**, 864 (1969).
[12] J. B. Goodenough, Phys. Rev. B **5**, 2764 (1972).
[13] L. M. Huisman, A. E. Carlsson, C. D. Gelatt Jr., and H. Ehrenreich, Phys. Rev. B **22**, 991 (1980).
[14] V. A. Gubanov, A. L. Ivanovsky, G. P. Shveikin, and D. E. Ellis, J. Phys. Chem. Solids **45**, 719 (1984).
[15] J. K. Burdett and T. Hughbanks, J. Am. Chem. Soc. **106**, 3101 (1984).
[16] J. Redinger, R. Eibler, P. Herzig, A. Neckel, R. Podloucky, and E. Wimmer, J. Phys. Chem. Solids **46**, 383 (1985).
[17] J. Redinger, R. Eibler, P. Herzig, A. Neckel, R. Podloucky, and E. Wimmer, J. Phys. Chem. Solids **47**, 387 (1986).
[18] P. Herzig, J. Redinger, R. Eibler, and A. Neckel, J. Solid State Chem. **70**, 281 (1987).
[19] F. Schlapansky, P. Herzig, R. Eibler, G. Hobiger, and A. Neckel, Z. Phys. B **75**, 187 (1989).
[20] G. Hobiger, P. Herzig, R. Eibler, F. Schlapansky, and A. Neckel, J. Phys.: Condens. Matter **2**, 4595 (1990).
[21] S. R. Barman and D. D. Sarma, Phys. Rev. B **49**, 16 141 (1994).
[22] C. Leung, M. Weinert, P. B. Allen, and R. M. Wentzcovitch, Phys. Rev. B **54**, 7857 (1996).
[23] D. Watanabe, O. Terasaki, A. Jostsons, and J. R. Castles, *The Chemistry of Extended Defects in Non-metallic Solids*, edited by L. Eyring and M. O'Keeffe (North-Holland, Amsterdam, 1970), p. 238.
[24] M. D. Banus, T. B. Reed, and A. J. Strauss, Phys. Rev. B **5**, 2775 (1972).
[25] K. Ichikawa, O. Terasaki, and T. Sagawa, J. Phys. Soc. Jpn. **36**, 706 (1974).
[26] G. K. Wertheim and D. N. E. Buchanan, Phys. Rev. B **17**, 2780 (1978).
[27] V. E. Henrich, H. J. Zeiger, and T. B. Reed, Phys. Rev. B **17**, 4121 (1978).
[28] M. V. Kuznetsov, J. F. Zhuravlev, V. A. Zhilyaev, and V. A. Gubanov, J. Electron Spectrosc. Relat. Phenom. **58**, 1 (1992).
[29] J. E. Holliday, *Soft X-ray Band Spectra*, edited by D. J. Fabian (Academic Press, New York, 1968), p. 101.
[30] I. A. Brytov, M. A. Rumsh, and A. S. Parobets, Fiz. Tverd. Tela **10**, 794 (1968) [Sov. Phys. Solid State **10**, 621 (1968)].
[31] D. W. Fischer, J. Appl. Phys. **41**, 3561 (1970).
[32] D. W. Fischer, *Band Structure Spectroscopy of Metals and Alloys*, edited by D. J. Fabian and L. M. Watson (Academic Press, New York, 1973), p. 669.
[33] K. Tsutsumi, O. Aita, and K. Ichikawa, Phys. Rev. B **15**, 4638 (1977).
[34] A. Taylor and N. J. Doyle, High Temp.-High Press. **1**, 679 (1969).
[35] M. D. Banus, Mater. Res. Bull. **2**, 563 (1967).
[36] M. D. Banus and T. B. Reed, *The Chemistry of Extended Defects in Nonmetallic Solids*, edited by L. Eyring and M. O'Keeffe (North-Holland, Amsterdam, 1970), p. 488.
[37] N. J. Doyle, J. K. Hulm, C. K. Jones, R. C. Miller, and A. Taylor, Phys. Lett. **26A**, 604 (1968).
[38] J. L. Murray and H. A. Wriedt, Bull. Alloy Phase Diagrams **8**, 148 (1987).
[39] After two years no change in the lattice structure or lattice parameter was found.
[40] TAP: artificial thallium acid phthalate ($C_8H_5O_4Tl$) crystal.
[41] E. Z. Kurmaev, V. V. Fedorenko, S. N. Shamin, A. V. Postnikov, G. Wiech, and Y. Kim, Phys. Scr. **T41**, 288 (1992).
[42] V. E. Dolgih, V. M. Cherkashenko, E. Z. Kurmaev, D. A. Goganov, E. K. Ovchinnikov, and Y. M. Yarmoshenko, Nucl. Instrum. Methods Phys. Res. A **224**, 117 (1984).

[43] V. E. Henrich, G. Dresselhaus, and H. J. Zeiger, Phys. Rev. Lett. **36**, 1335 (1976).
[44] W. Göpel, G. Rocker, and R. Feierabend, Phys. Rev. B **28**, 3427 (1983).
[45] W. Göpel, J. A. Anderson, D. Frankel, M. Jaehnig, K. Phillips, J. A. Schäfer, and G. Rocker, Surf. Sci. **139**, 333 (1984).
[46] T. Choudhury, S. O. Saied, J. L. Sullivan, and A. M. Abbot, J. Phys. D **22**, 1185 (1989).
[47] S. Munnix and M. Schmeits, Phys. Rev. B **30**, 2202 (1984).
[48] V. M. Cherkashenko, V. V. Shumilov, V. R. Galakhov, M. Y. Khodos, N. V. Krivosheev, S. N. Nemnonov, E. Z. Kurmaev, and V. A. Gubanov, Izv. Akad. Nauk SSSR, Neorg. Mater. **23**, 96 (1987) [Inorg. Mater. **23**, 80 (1987)].
[49] F. M. Michel-Calendini, J. Phys. Chem. Solids **35**, 1163 (1974).
[50] D. W. Fischer and W. L. Baun, J. Appl. Phys. **39**, 4757 (1968).
[51] J. J. Yeh and I. Lindau, At. Data Nucl. Data Tables **32**, 1 (1985).
[52] A. E. Bocquet, T. Mizokawa, K. Morikawa, A. Fujimori, S. R. Barman, K. Maiti, D. D. Sarma, Y. Tokura, and M. Onoda, Phys. Rev. B **53**, 1161 (1996).
[53] J. Zaanen, G. A. Sawatzky, and J. W. Allen, Phys. Rev. Lett. **55**, 418 (1985).
[54] R. Ahuja, O. Eriksson, J. M. Wills, and B. Johansson, Phys. Rev. B **53**, 3072 (1996).
[55] A. Fujimori, I. Hase, H. Namatame, Y. Fujishima, Y. Tokura, H. Eisaki, S. Uchida, K. Takegahara, and F. M. F. de Groot, Phys. Rev. Lett. **69**, 1796 (1992).
[56] I. H. Inoue, I. Hase, Y. Aiura, A. Fujimori, Y. Haruyama, T. Maruyama, and Y. Nishihara, Phys. Rev. Lett. **74**, 2539 (1995).